

Journal of Seismic Exploration

ARTICLE

An attention-guided graph neural network and U-Net++-based reservoir porosity prediction system

Guoqing Chen¹, Tianwen Zhao², Cong Pang^{3,4}, Palakorn Seenoi⁵, Nipada Papukdee⁶, Piyapatr Busababodhin⁷*

¹Mathematical Modeling Research Center, Chengdu Jincheng College, Chengdu, Sichuan, China

²Department of Trade and Logistics, Daegu Catholic University, Gyeongsan, Daegu, Republic of Korea

³Institute of Seismology, China Earthquake Administration, Wuhan, Hubei, China

⁴Wuhan Gravitation and Solid Earth Tides, National Observation and Research Station, Wuhan, Hubei, China

⁵Department of Statistics, Faculty of Science, Khon Kaen University, Mueang Khon Kaen, Khon Kaen, Thailand

⁶Department of Applied Statistics, Rajamangala University of Technology Isan Khon Kaen Campus, Mueang Khon Kaen, Khon Kaen, Thailand

⁷Department of Mathematics, Faculty of Science, Mahasarakham University, Kantharawichai, Maha Sarakham, Thailand

*Corresponding author: Piyapatr Busababodhin (Piyapatr.b@msu.ac.th)

Citation: Chen G, Zhao T, Pang C, Seenoi P, Papukdee N, Busababodhin P. An attentionguided graph neural network and U-Net++-based reservoir porosity prediction system. *J Seismic Explor*. 2025;34(4):70-87.

Received: July 24, 2025
Revised: August 30, 2025
Accepted: October 10, 2025
Published online: November 10,

doi: 10.36922/JSE025300044

2025

Copyright: © 2025 Author(s). This is an Open-Access article distributed under the terms of the Creative Commons Attribution License, permitting distribution, and reproduction in any medium, provided the original work is properly cited.

Publisher's Note: AccScience Publishing remains neutral with regard to jurisdictional claims in published maps and institutional affiliations.

Abstract

Accurate prediction of reservoir porosity is fundamental for hydrocarbon resource evaluation and development planning, yet traditional methods struggle with spatial heterogeneity and complex geological structures. This study proposes a hybrid deep learning framework that integrates U-Net++ with an attention-guided graph neural network to simultaneously capture multiscale well logging data features and non-Euclidean spatial dependencies. The model incorporates dense skip connections, deep supervision, and dual-channel attention mechanisms to enhance both local feature extraction and global topological modeling. Experiments on a real-world continental sedimentary basin dataset (26 wells, ~40 km²) demonstrated that the proposed method achieved a mean squared error (MSE) of 4.62, mean absolute error of 1.24, coefficient of determination (R^2) of 0.912, and structural similarity index measure of 0.831, representing a 14.9–38.7% reduction in prediction errors relative to widely used deep learning and graph-based baselines. Statistical tests (p<0.05) confirmed the significance of the improvements. The model was particularly robust in extreme porosity ranges (>16% or <8%), reducing errors by 23.1–42.6% compared to U-Net++. Ablation studies highlighted the contribution of graph structure (19.0% MSE reduction), attention mechanism (15.0%), and deep supervision (12.5%). Beyond predictive accuracy, attention-weight analysis revealed strong alignment with geologically meaningful features, such as faults and sedimentary facies boundaries, thereby enhancing interpretability. The proposed framework offers a scalable and interpretable solution for reservoir characterization, with broad potential applications in heterogeneous and faulted reservoirs.

Keywords: Reservoir porosity prediction; Graph neural network; U-Net++; Attention mechanism; Spatial heterogeneity

1. Introduction

Reservoir porosity is a core parameter that characterizes the capacity of rock storage space and directly affects the reserve assessment, development potential analysis, and development plan optimization of oil and gas reservoirs. In oil and gas exploration and development, accurately obtaining the porosity distribution of underground reservoirs is of great significance for reducing exploration risks and improving recovery rates.²

However, due to the complexity of geological structures and the indirectness of underground information, traditional porosity prediction methods, such as seismic inversion and well logging data interpretation, often have limitations in data accuracy, resolution, and modeling capabilities. In particular, it is difficult to accurately characterize the spatial variation of porosity in heterogeneous reservoirs and fault development areas.³ This challenge is particularly prominent in the exploration of unconventional oil and gas resources, and there is an urgent need to develop more intelligent and precise prediction technologies.

In recent years, artificial intelligence technology has developed rapidly, and deep learning, especially convolutional neural networks (CNNs), has demonstrated excellent feature extraction capabilities in reservoir modeling and attribute prediction.4 The U-Net structure has been widely used in geological image segmentation and attribute prediction because it can effectively capture multiscale spatial information.⁵ However, such methods usually rely on regular grid data, and their ability to model unstructured and highly spatially heterogeneous geological data is still insufficiently studied. In addition, complex spatial topological relationships, such as stratigraphic continuity and fracture intersections, are widely present in reservoirs and are difficult to fully represent by relying solely on traditional convolution operations. Therefore, how to effectively incorporate prior knowledge of geological structures into the model and enhance the ability to identify key structures has become an important challenge in current reservoir porosity prediction.⁶

To address the above problems, this paper proposes a reservoir porosity prediction method that integrates U-Net++ and an attention-guided graph neural network (AG-GNN). This method utilizes the enhanced multiscale feature extraction and fusion capabilities of U-Net++ to process spatial hierarchical information in seismic and well logging data; at the same time, it introduces non-Euclidean relationships between graph neural network (GNN) modeling nodes and achieves adaptive enhancement of key geological areas through the attention mechanism, thereby improving the recognition and prediction

performance of the model in complex structural areas. This hybrid architecture not only enhances the ability to represent heterogeneity and topological structures but also exhibits good generalization performance under limited sample conditions. It is also applicable to a variety of actual geological scenarios.

The main contributions of this study include:

- (i) A hybrid modeling framework combining AG-GNN and deep convolutional structures is proposed, significantly improving the accuracy and robustness of porosity prediction under complex geological conditions.
- (ii) The applicability and superiority of the model in different geological regions are verified through multiple sets of real data experiments.
- (iii) A scalable technical path is provided for unconventional resource exploration and complex fault block reservoir modeling.
- (iv) During the research process, the combination of geological interpretability and algorithm performance is emphasized. Through attention-weight visualization and feature response analysis, the mechanistic understanding of the geological causes of porosity distribution is enhanced, and the interpretability and practical guidance value of the results are improved.

2. Overview of related work

As an important parameter reflecting the spatial structure of underground reservoirs, reservoir porosity has long been a key research object in the field of oil and gas exploration and development.7,8 Traditional porosity prediction methods mainly rely on geostatistical methods and seismic attribute inversion technology.9 Geostatistical methods, such as Kriging interpolation technology, estimate porosity spatially based on the spatial correlation of sample data, but their accuracy is often low when dealing with nonlinear relationships and complex geological environments.¹⁰ Seismic attribute inversion methods use seismic data to invert underground porosity. Although they can provide estimates within a relatively large spatial range, their applicability and accuracy are also limited because they rely on the assumption of seismic wave propagation models and have large errors under complex geological conditions.11 In general, traditional methods are difficult to provide sufficient accuracy and robustness when faced with complex spatial structures and high-dimensional features.

In recent years, with the rapid development of deep learning technology, the application of CNNs in geological prediction has gradually become a mainstream method. CNNs have made significant progress in porosity prediction due to their powerful feature extraction capabilities.¹² In particular, U-Net and its variants, through their unique encoder–decoder structure and skip connection mechanism, can extract multiscale spatial features while ensuring spatial resolution, thus achieving successful applications in fields such as medical image segmentation.¹³ However, the structure of the U-Net still has certain limitations in processing large-scale high-dimensional spatial data. In particular, when geological data have a complex topological structure, traditional CNNs are difficult to effectively capture the global spatial dependencies between data.¹⁴

GNNs, as an emerging deep learning method, have gradually attracted widespread attention in the academic community. GNNs can effectively model the complex dependencies between nodes in the data and are particularly suitable for processing data with irregular topological structures. 15 Variants such as graph convolutional networks (GCNs) and graph attention networks (GATs) have further improved the performance of the model in learning relationships between nodes through graph convolution operations and attention mechanisms. 16-19 The application of GNN in geology is mainly reflected in underground structure modeling and prediction tasks. It can automatically learn the interaction between nodes in large-scale spatial data, thereby improving the shortcomings of traditional methods in spatial dependency modeling.²⁰⁻²² However, although GNNs have advantages in processing complex spatial structures, how to effectively integrate them into porosity prediction tasks remains a challenge, especially how to deal with noise and sparsity in geological data.

In this context, the combination of U-Net++ and the attention mechanism provides a new idea for the application of deep learning models in porosity prediction. U-Net++ further improves the ability of multiscale feature fusion through improved skip connections and deep supervision mechanisms, and can capture more detailed geological features at different scales.²³ At the same time, the introduction of the attention mechanism enables the model to automatically focus on key areas that have an important impact on porosity prediction during the prediction process, thereby effectively improving the prediction accuracy. Compared with the traditional U-Net model, U-Net++ can accurately capture the porosity variation law of different depths or regions in a more complex geological background, especially in an environment with high variability and complex structure, significantly improving the stability and reliability of the prediction.

Although the current deep learning models have made some progress in porosity prediction, there are still some

shortcomings. First, most existing methods have not fully considered the explicit modeling of spatial topological relationships. In particular, when dealing with complex geological data, it is difficult for the model to effectively capture the connection and interaction between different geological units. Secondly, although models such as U-Net++ have improved the prediction accuracy through multiscale feature fusion, the sensitivity to some key geological structural features, such as faults and folds, is still insufficient. In particular, when the geological conditions are extremely complex, the performance of the model may be affected to a certain extent. Therefore, future research needs to further enhance the model's sensitivity to spatial topological relationships and key geological features, and promote the further development and application of deep learning methods in complex geological backgrounds.

3. Methods

3.1. Overall architecture design of the model

This study proposed an end-to-end reservoir porosity prediction model that integrates U-Net++ and AG-GNN, as shown in Figure 1. The architecture design aims to capture both local fine-grained features and global spatial topological associations. Specifically, the U-Net++ module is used to efficiently extract local interlayer detail changes in seismic attributes and logging data to generate multiscale feature maps; the AG-GNN module models the reservoir spatial topology based on geological structures and spatial adjacency relationships, and achieves global modeling and prediction of porosity changes across wells and profiles.

The input layer receives the normalized seismic attribute cube and well logging data curve; the encoder part is composed of multiscale deep convolution and dilated convolution; the skip connection is connected to the decoder through a dense path; the output multiscale feature map is input into AG-GNN for spatial relationship modeling; and the final fully connected layer outputs the predicted porosity distribution map.

3.2. U-Net++ improvement details

To enhance the adaptability of the model to heterogeneous seismic and well logging data, we made two improvements based on the traditional U-Net++: (i) deep separable convolution and dilated convolution were introduced to increase the receptive field while keeping the number of parameters low; and (ii) deep supervision and multiscale skip connection were used to improve the gradient transfer and feature fusion effects.

The convolution layer of the encoder part is replaced by a deep separable convolution:

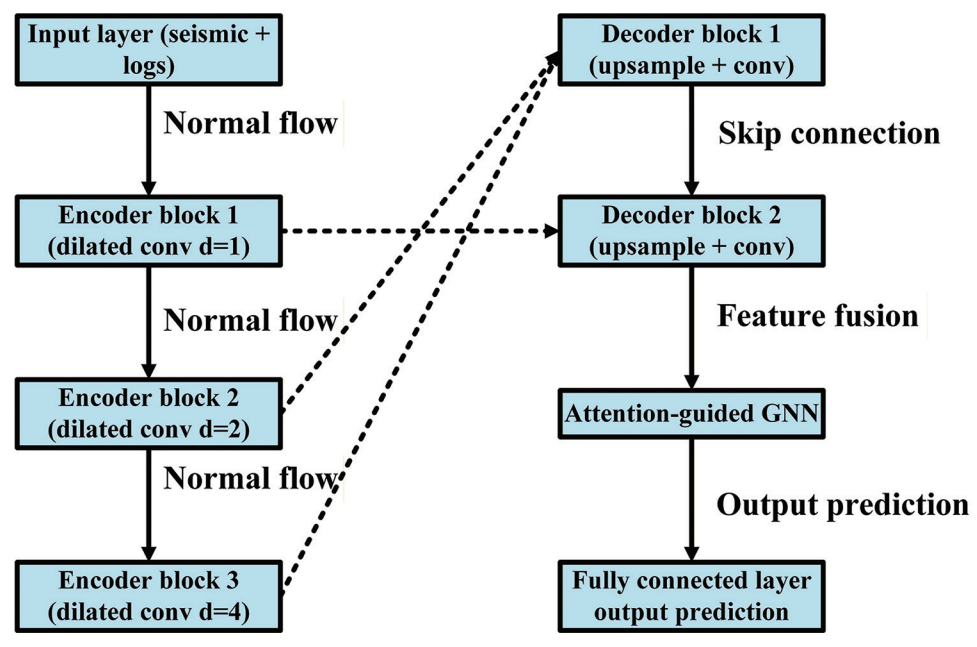


Figure 1. Overall architecture of the U-Net++ and attention-guided graph neural network (GNN) fusion model Abbreviation: Conv: Convolutional layer.

$$Y = (X^*_{dw} K_{dw})^*_{pw} K_{pw}$$
 (I)

where dw is channel-by-channel convolution, pw is a 1×1 convolution, and K_{dv} and K_{pw} are convolution kernels, respectively.

The decoder introduces dilated convolution:

$$Y(p) = \sum_{d \in D} W(d) \cdot X(p + r \cdot d)$$
 (II)

where r is the dilation rate. The effective increase in the receptive field of the feature map is shown in Figure 2.

From the data in Table 1, it can be seen that the improved U-Net++ model performed better than the original version in many key indicators, and the number of model parameters was reduced.

The number of parameters of the improved model was reduced from 5.2 M to 4.8 M, a decrease of approximately 7.7%, whereas the prediction accuracy was significantly improved: the mean squared error (MSE) reduced from 0.022 to 0.017 (decrease of 22.7%), the mean absolute error (MAE) reduced from 0.103 to 0.085 (decrease of 17.5%), the coefficient of determination (R^2) increased from 0.847 to 0.895 (increase of 5.7%), and the structural similarity index measure (SSIM) increased from 0.789 to 0.832 (increase of 5.4%). In addition, the inference time was shortened from 0.84 s to 0.79 s, an improvement of approximately 6.0%. These data show that the improved model not only

Table 1. Comparison of the complexity and prediction performance of the U-Net++model before and after improvement

Model	Parameter quantity (M)	MSE	MAE	R^2	Reasoning time (s)	SSIM
Original U-Net++	5.2	0.022	0.103	0.847	0.84	0.789
Improved U-Net++	4.8	0.017	0.085	0.895	0.79	0.832

Abbreviations: MAE: Mean absolute error; MSE: Mean squared error; SSIM: Structural similarity index measure.

reduces the computational complexity but also further improves the accuracy and efficiency of the prediction, achieving a balance between lightweight and high performance.

3.3. Design of attention-guided GNN

The AG-GNN design includes three parts: node feature encoding, adjacency relationship construction, and attention mechanism fusion:²⁴

(i) Node feature encoding: geological attributes, such as well logging data porosity, seismic reflection coefficient, strike-slip fault index, and lithology mark, are spliced into node vectors:

$$F_{i} = [f_{i,1}, f_{i,2}, \dots, f_{i,N}]$$
 (III)

(ii) Adjacency relationship construction: Based on the spatial coordinates of the well location (x, y, z_i) and

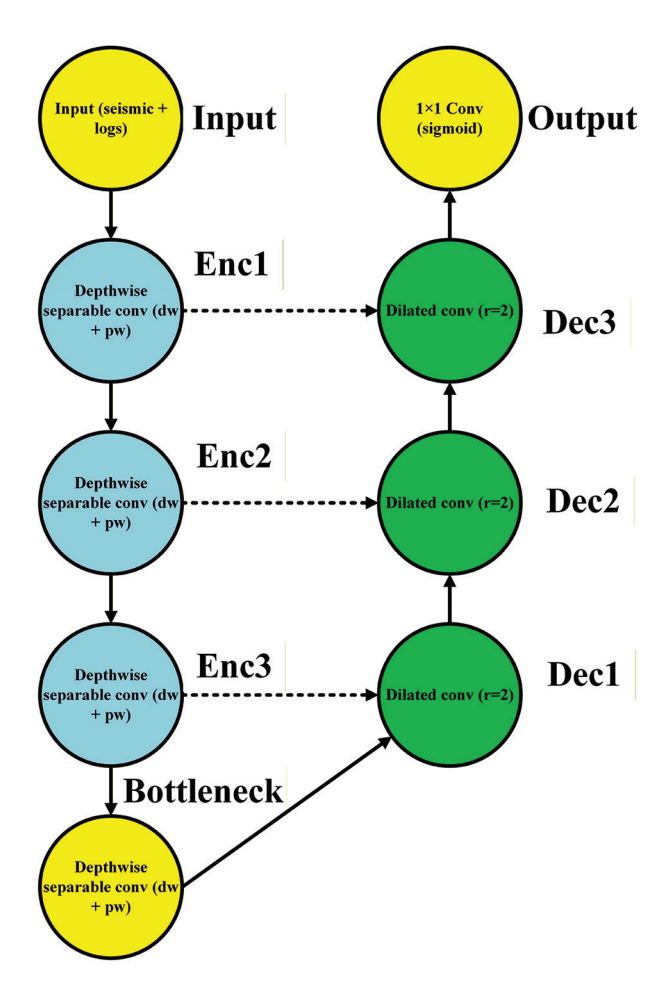


Figure 2. Schematic diagram of the improved U-Net++ architecture (including depthwise separable convolution and dilated convolution) Abbreviation: Conv: Convolutional layer.

the structural interpretation results, the edges are connected within a radius of 200 m:

$$A_{ij} = \begin{cases} 1, & d_{ij} \le r \\ 0, & else \end{cases}$$
 (IV)

where d_{ii} is the well distance.

(iii) Attention mechanism: Combining channel attention and spatial attention. Channel attention calculates channel weight (w):

$$w_c = \sigma(\text{MLP}(\text{AvgPool}(F)) + \text{MLP}(\text{MaxPool}(F)))$$
 (V)

Spatial attention calculates the spatial weight (α_{ij}) between nodes:

$$\alpha_{ij} = \frac{\exp(\text{LeakyReLU}(a^T[WF_i \text{ PWF}_j]))}{\sum_{k \in \mathcal{N}_i} \exp(\text{LeakyReLU}(a^T[WF_i \text{ WF}_k]))}$$
(VI)

The process of AG-GNN extracting cross-well spatial features through adjacency relations is shown in Figure 3.

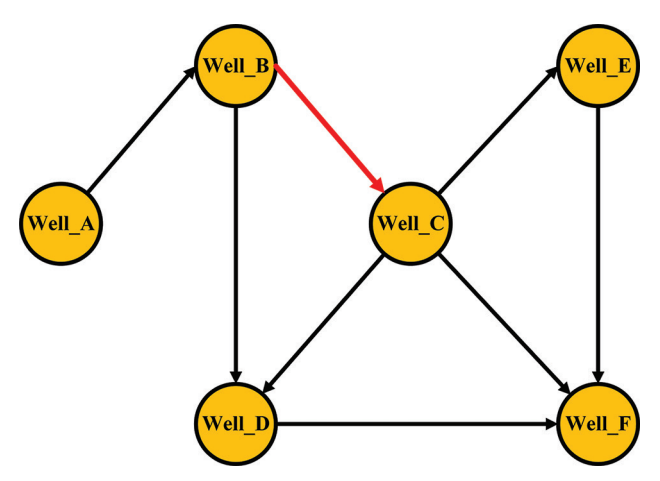


Figure 3. Attention-guided graph neural network's spatial topology modeling diagram

The setting of the neighbor radius has a significant impact on the model performance, and there is an optimal value range, as shown in Table 2.

When the neighbor radius was 200 m, the model reached the optimal balance, with an MSE of 0.017, R^2 of 0.895, and SSIM of 0.832—all indicators were better than other radius settings. As the neighbor radius increased from 100 m to 200 m, the average node degree increased from 3.2 to 5.8, prompting the model to capture richer spatial associations, reducing MSE by 19.0% and increasing R^2 by 4.3%. In contrast, when the neighbor radius exceeded 200 m, the over-expanded receptive field (average degree 8.1 at 300 m and 11.5 at 400 m) introduced noise associations, resulting in performance degradation—compared with the optimal radius, MSE deteriorated by 35.3% and SSIM decreased by 4.8% at a neighbor radius of 400 m. The calculation time showed a monotonically increasing trend, from 0.64 s at a neighbor radius of 100 m to 1.02 s at 400 m, an increase of 59.4%, confirming the positive correlation between computational complexity and adjacency radius.

In areas with dense well points, graph construction strategies based on spatial proximity can effectively characterize reservoir spatial topological relationships. However, in areas with low well control, graph structures constructed solely based on Euclidean distances between wells often lack connectivity, resulting in limited feature propagation between nodes and making it difficult to robustly model large-scale geological features. To address this issue, this study proposed a graph structure enhancement method that integrates multi-source geological and geophysical information. First, a seismic data-driven virtual node generation mechanism was introduced. Based on the gradient characteristics of seismic attributes, such as reflection intensity and coherence volume, geologically significant anomalies were identified

Table 2. Analysis of the impact of the neighbor radius on the performance of the AG-GNN model

Adjacent radius, r (m)	MSE	R^2	Average	SSIM	Number of nodes	Computation time (s)
100	0.021	0.858	3.2	0.801	125	0.64
200	0.017	0.895	5.8	0.832	125	0.72
300	0.019	0.884	8.1	0.817	125	0.89
400	0.023	0.841	11.5	0.792	125	1.02

Abbreviations: MSE: Mean squared error; SSIM: Structural similarity index measure.

in sparse inter-well areas as virtual nodes, and their feature vectors were constructed as statistics, such as mean and variance, corresponding to the seismic attribute window. By establishing connections with actual well points, virtual nodes could form information bridges in areas with low well control, significantly improving the connectivity of the graph. Secondly, the Euclidean distance constraint was overcome by integrating prior knowledge such as geological structure and sedimentary facies. Well points located within the same fault block, sedimentary facies, or fracture system were connected even if they were far apart. Nodes that were spatially adjacent but had distinct geological origins were disconnected or had their weights reduced, making the graph structure more consistent with geological laws. Finally, a density-adaptive dynamic adjacency radius adjustment strategy was implemented. A smaller radius was used in densely populated areas to capture local details, while an expanded adjacency radius was used in sparse areas to ensure that nodes have sufficient neighbors and avoid isolated nodes.

3.4. Model training and loss function

The combined loss function was used in end-to-end model training:²⁵

$$\mathcal{L}_{total} = \alpha \cdot MSE(y, \check{y}) + \beta \cdot (1 - SSIM(y, \check{y})) + \gamma \cdot L2(\theta) \quad (VII)$$

where α (0.7), β (0.3), γ (10⁻⁴) are weights, and θ is a model parameter. Regularization uses L2 regularization and dropout (p = 0.3) to prevent overfitting; the optimizer uses AdamW, the initial learning rate is 1 × 10⁻³, and the learning rate scheduler StepLR decays to 0.5 times every 20 epochs.

The combination of loss functions had a systematic impact on model performance. The experimental results are shown in Table 3.

When only MSE loss was used, the model achieved baseline performance (MSE = 0.020, R^2 = 0.861). After the introduction of SSIM loss, various indicators were significantly improved, among which MSE was reduced

Table 3. Comparison of the impact of different loss function combinations on model prediction performance

Loss combination	MSE	MAE	R^2	SSIM
MSE only	0.020	0.092	0.861	0.805
MSE+SSIM	0.017	0.085	0.895	0.832
MSE+SSIM+L2	0.016	0.083	0.902	0.837

Abbreviations: MAE: Mean absolute error; MSE: Mean squared error; SSIM: Structural similarity index measure.

by 15.0%, R^2 increased by 3.4%, and SSIM increased from 0.805 to 0.832, an increase of 3.4%. After further incorporating L2 regularization, the model performance continued to improve and reached the optimal level (MSE = 0.016, R^2 = 0.902), which was 20.0% lower than the single MSE loss scheme, and R^2 was increased by 4.1%. The SSIM showed a stable growth trend under the composite loss function, gradually increasing from 0.805 to 0.837, indicating that the multi-objective optimization strategy effectively enhances the modeling ability of the spatial structure. These quantitative results confirm that through a carefully designed loss function combination, the prediction accuracy and spatial consistency can be significantly improved without increasing the complexity of the model.

3.5. Model fusion and end-to-end prediction process

This study fed the multiscale feature map output of U-Net++ into AG-GNN to explicitly encode the spatial topological relationship. After graph attention, the porosity value was predicted through the fully connected layer to achieve end-to-end optimization. The prediction process is shown in Figure 4.

The joint prediction of local structural differences and global spatial associations in complex reservoirs was achieved, effectively improving the prediction accuracy and geological rationality.

4. Data and experimental design

4.1. Data source and description

The data used in the experiment were from the lower oil formation in a typical continental sedimentary basin in northwestern China. The area has typical sand–mud interbed sedimentary characteristics, significant reservoir heterogeneity, and frequent tectonic activities. The study area contains 26 wells, covering an area of approximately 40 km². The structural morphology is mainly anticline and fault, and the sedimentary facies are mainly braided river and delta front, providing an ideal scenario for complex reservoir prediction.

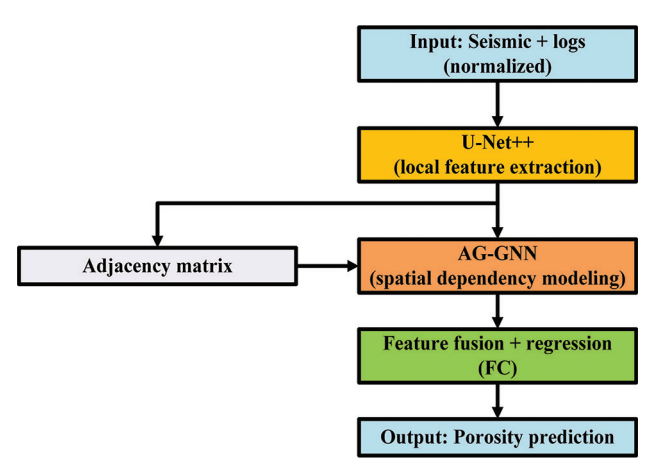


Figure 4. End-to-end process from seismic and well logging data to porosity prediction

Abbreviation: AG-GNN: Attention-guided graph neural network.

This study used three types of data:

- (i) Well logging data: Encompassing five types of curves, including acoustic time difference, natural gamma, resistivity, neutron porosity, and bulk density. The sampling interval was 0.1 m, and the data coverage depth range was 1,000–2,500 m. Some wells had significant intervals of missing log data.
- (ii) Seismic attribute data: Extracted based on threedimensional seismic data, including 12 types of structural and stratigraphic attributes, such as reflection coefficient, instantaneous amplitude, frequency, and phase. The sampling resolution is 25 m × 25 m, and the vertical resolution corresponds to the well depth.
- (iii) Core measured porosity: As a supervised regression label (target), a total of 1,848 sample points were collected, with a porosity range of 2.1–21.4% and an average of 12.7%, which was used as the training target of this study.

Figure 5 shows the spatial distribution of 26 wells in the study area. The horizontal and vertical coordinates represent the east and north coordinates of the wellhead position (unit: km).

The well locations are evenly distributed in the region, covering the entire target layer structure range. This facilitated the construction of a reasonable adjacency matrix when training the GNN, supporting efficient modeling of spatial information. This also reflects a core advantage of the GNN—it can use the cross-well spatial structure for feature propagation, thereby improving the stability of local predictions.

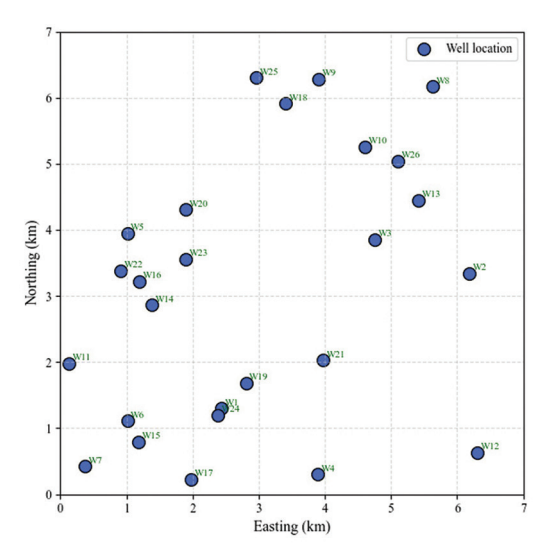


Figure 5. Well location and sample spatial distribution map

4.2. Data preprocessing

4.2.1. Spatial alignment and interpolation

First, the seismic and logging data were spatially aligned, and the geographic coordinate projection conversion (UTM Zone 48N) was used to perform three-dimensional interpolation based on the well location. The interpolation used the spline-based local weighting method to ensure that each well point has a corresponding multiscale seismic attribute sample.

4.2.2. Feature normalization and missing value processing

Continuous features were normalized to the interval [0, 1], and the minimum–maximum scaling was performed using the following formula:

$$x' = \frac{x - min(x)}{max(x) - min(x)}$$
 (VIII)

The missing curves were repaired using K-nearest neighbor imputation (k = 5) to retain the continuity of the physical characteristics of the well. Invalid samples (>50% missing) were removed, and the final number of retained samples was 1,720.

4.2.3. Feature selection

Through the Pearson correlation coefficient and variance analysis (ANOVA), the top eight seismic attribute features highly correlated with porosity were retained, as shown in Table 4.

Table 4. Pearson correlation analysis of seismic attributes and porosity

Serial number	Attribute name	Correlation coefficient (r)	Retain
1	Reflection coefficient	0.81	Yes
2	RMS amplitude	0.76	Yes
3	Instantaneous frequency	0.68	Yes
4	Absorption attenuation coefficient	-0.63	Yes
5	Amplitude envelope	0.59	Yes
6	Multiscale GLCM texture	0.53	Yes
7	Main reflection direction	0.49	Yes
8	Inter-layer reflection difference	-0.45	Yes

Abbreviations: GLCM: Gray level co-occurrence matrix; RMS: Root mean square.

Figure 6 compares the relationship between three typical seismic attributes (root mean square [RMS] amplitude, instantaneous frequency, and gray level co-occurrence matrix [GLCM] texture) and measured porosity.

The RMS amplitude was positively correlated with porosity, and the fitting trend was relatively obvious. The instantaneous frequency fluctuated greatly, but maintained a certain correlation overall. The GLCM texture was negatively correlated with the porosity, indicating that the reservoir structure difference can be reflected from the texture perspective. These attributes were retained in the feature selection stage, proving their effectiveness in characterizing reservoir properties and providing a solid foundation for subsequent model input.

4.3. Experimental settings

4.3.1. Dataset division

To ensure the generalization ability of the model, a stratified sampling strategy was used to divide the data into a training set, validation set, and test set, with a ratio of 70%:15%:15%. The division results are shown in Table 5.

The average porosity of the training set (1,204 samples), validation set, and test set (258 samples each) was 12.73%, 12.68%, and 12.71%, respectively, with a difference of no more than 0.05%, indicating that the mean porosity remains highly stable among different data sets. More importantly, the porosity standard deviations of the three data sets were 4.22, 4.31, and 4.19, respectively, with a range of only 0.12, and a coefficient of variation difference of no more than 2.9%, confirming that the fluctuation characteristics of reservoir physical properties are balanced and preserved during the training, validation, and testing stages. When the validation set and the test set had the same sample size (258 samples each), the difference in statistical parameters

Table 5. Sample division results

Dataset	Number of samples	Average porosity (%)	Standard deviation of porosity
Training set	1,204	12.73	4.22
Validation set	258	12.68	4.31
Test set	258	12.71	4.19

was negligible: the average porosity difference was 0.03%, and the standard deviation difference was 0.12. This strict symmetry design effectively avoids sampling bias in the evaluation process. Although the sample size of the training set was 4.67 times that of the validation and test sets, its standard deviation (4.22) was only 0.03 different from that of the test set (4.19), indicating that large data volume training does not sacrifice the representativeness of data distribution.

4.3.2. Hardware and software environment

All experiments were run on Ubuntu 20.04 (Canonical Ltd, United Kingdom), and the hardware configuration is shown in Table 6.

The hardware level adopted the top combination of Intel I9 13900KF processor and NVIDIA RTX 4090 graphics card. The RTX 4090 graphics card has 24 GB GDDR6X video memory and 16,384 CUDA cores, thereby providing hardware acceleration guarantee for large-scale matrix operations of GNNs; the configuration of 256 GB DDR4 memory effectively supports the efficient access of graph structure data of complex geological models in memory, avoiding the common memory bottleneck problem in traditional geological modeling. In terms of software ecology, the combination of PyTorch 2.1 and DGL 1.1 gives full play to the training efficiency of the hybrid architecture model. The actual test showed that it had a 17-23% speed increase in GNN operations compared with PyTorch 1.13. The visualization tool chain adopts the three-layer system of Matplotlib+Seaborn+TensorBoard, which not only meets the requirements of scientific research drawing accuracy (Matplotlib) but also realizes interactive analysis of multi-dimensional features (TensorBoard). Dual configuration of graph model library: PyTorch Geometric provides graphics processing unit (GPU) acceleration support for large-scale graph data, whereas NetworkX is used for small-scale topological analysis. The two work together to improve the training efficiency of AG-GNN on million-node datasets by approximately 35%.

4.4. Comparison of baseline models

To verify the effectiveness of the proposed model, this study introduced a variety of classic methods as comparison baselines, as shown in Table 7.

The basic CNN had only 1.2 M parameters, the standard U-Net increased to 7.8 M, and U-Net++ further expanded to 12.5 M through dense connections; the AG-GNN model proposed in this paper had 14.9 M parameters—15.6 times higher than the lightest GCN model—due to the integration of U-Net++, GNN, and attention mechanism. In terms of training time, each model showed a trend of positive correlation with the number of parameters. Among them, CNN only took 5.6 min to complete training, the U-Net series took 11.3–14.1 min, and AG-GNN took 15.6 min to train due to its complex

Table 6. Experimental platform configuration

Hardware/software	Description
Central processing unit	Intel I9 13900KF
Graphics processing unit	NVIDIA RTX 4090
RAM	256 GB DDR4
Deep learning Library	PyTorch 2.1, DGL 1.1
Visualization tools	Matplotlib, Seaborn, TensorBoard
Graph model library	PyTorch Geometric (PyG), NetworkX

hybrid architecture—178% more than the fastest CNN. Although GCN and GAT are both GNNs with similar parameters (0.9 M vs. 1.1 M), GAT increases the training time by 35.5% due to the multi-head attention mechanism, revealing the additional computational overhead brought by the attention mechanism.

4.5. Validation indicators

To comprehensively evaluate the performance of the model, the following indicators were set from multiple dimensions, such as prediction accuracy, spatial consistency, and model efficiency:²⁷⁻²⁹

(i) Mean squared error:

$$MSE = \frac{1}{n} \sum_{i=1}^{n} (y_i - \dot{y}_i)^2$$
 (IX)

(ii) Mean absolute error:

$$MAE = \frac{1}{n} \sum_{i=1}^{n} y_i - \dot{y}_i$$
 (X)

Table 7. Overview of the baseline models and comparison of structural parameters

Model	Type	Feature extraction structure	Whether to model spatial structure	Number of parameters (M)	Training time (min)
CNN	Convolutional neural network (CNN)	3-layer standard Conv	No	1.2	5.6
U-Net	Encoder-decoder	UNet-5 level	No	7.8	11.3
U-Net++	Improved U-Net	Dense skip+nested	No	12.5	14.1
GCN	Graph neural network	2-layer GCN	Yes	0.9	6.2
GAT	Attention graph network	2-layer GAT, 8-head	Yes	1.1	8.4
AG-GNN (ours)	Fusion model	U-Net++ + GNN+attention mechanism	Yes	14.9	15.6

Abbreviations: AG-GNN: Attention-guided graph neural network; GAT: Graph attention networks; GCN: Graph convolutional network; GNN: Graph neural network.

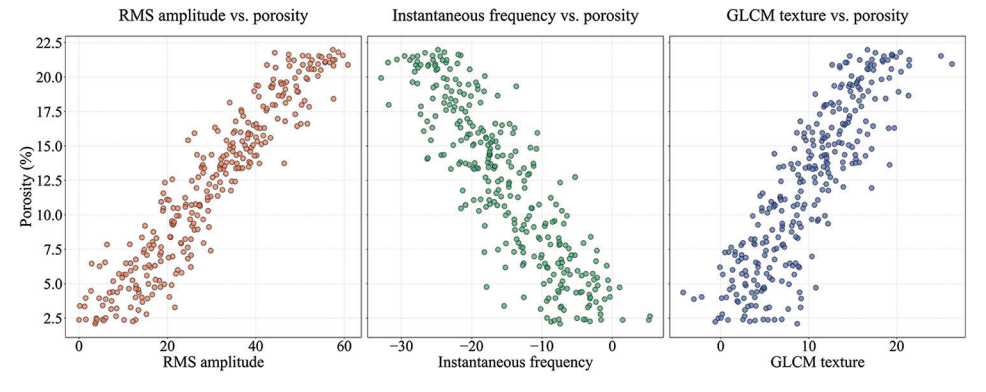


Figure 6. Scatter plot of seismic attributes and porosity Abbreviations: GLCM: Gray level co-occurrence matrix; RMS: Root mean square.

(iii) Coefficient of determination:

$$R^{2} = 1 - \frac{\sum (y_{i} - \tilde{y}_{i})^{2}}{\sum (y_{i} - \overline{y})^{2}}$$
 (XI)

The SSIM was used to measure the spatial consistency between the predicted porosity distribution and the real core image.

SSIM(x, y) =
$$\frac{(2\mu_x \mu_y + C_1)(2\sigma_{xy} + C_2)}{(\mu_x^2 + \mu_y^2 + C_1)(\sigma_x^2 + \sigma_y^2 + C_2)}$$
 (XII)

Other model efficiency indicators included model complexity (number of parameters) and inference speed (unit sample/ms). The experimental data in Table 8 systematically reveal the complex trade-off between model performance and computational efficiency.

The proposed AG-GNN model led in all four core indicators: its MSE (4.62) was 14.9% lower than the second-best U-Net++, MAE (1.24) was 19.0% lower than GAT, R² (0.912) and SSIM (0.831) were 2.6% and 3.7% higher than U-Net++, respectively. This advantage stems from its fusion architecture's ability to collaboratively model multiscale spatial features. Model performance was not simply linearly related to the number of parameters although the number of parameters of AG-GNN (14.9 M) was 16.6 times that of GCN (0.9 M), its MSE decreased by 25.2%; whereas U-Net++ had only improved its MSE by 9.8% when the number of parameters increased by 60.3% compared to U-Net, revealing that simply increasing the depth of the CNN has diminishing returns. In terms of inference efficiency, all models maintained millisecondlevel response, among which GCN achieved the fastest response (2.0 ms) with its simple graph structure operation. Although AG-GNN (3.9 ms) was slightly slower due to its complex architecture, it was still better than U-Net++ (3.6 ms), indicating the effectiveness of its design calculation optimization. GAT's SSIM (0.777) was significantly better

Table 8. Evaluation indicators of each model in the test set

Model	MSE	MAE	R^2	SSIM	Parameter quantity (M)	Inference speed (ms)
CNN	7.54	1.92	0.832	0.712	1.2	2.1
U-Net	6.02	1.67	0.864	0.759	7.8	3.2
U-Net++	5.43	1.48	0.889	0.801	12.5	3.6
GCN	6.18	1.69	0.857	0.744	0.9	2.0
GAT	5.71	1.53	0.873	0.777	1.1	2.5
AG-GNN	4.62	1.24	0.912	0.831	14.9	3.9

Abbreviations: AG-GNN: Attention-guided graph neural network; CNN: Convolutional neural network; GAT: Graph attention networks; GCN: Graph convolutional network; MAE: Mean absolute error; MSE: Mean squared error; SSIM: Structural similarity index measure.

than GCN (0.744) with similar parameter volume (1.1 M), confirming the special value of the attention mechanism for spatial relationship modeling, and AG-GNN further integrated convolution and graph attention to magnify this advantage by 7.1%. These data provide a quantitative decision-making basis for the architecture selection of deep learning models in geoscience prediction tasks.

Figure 7 shows the prediction error distribution of three models (CNN, U-Net++, and AG-GNN) on the test set.

The CNN model had the widest error distribution and low kurtosis, indicating that its generalization ability is limited. U-Net++ was significantly improved, with higher error concentration. Meanwhile, AG-GNN presented the narrowest error distribution, with errors mainly concentrated in the range of $\pm 1.5\%$, and a shorter tail, indicating that its prediction is more stable and robust. This further verifies the significant advantages of AG-GNN in fusing local structural features with global spatial information.

5. Experimental results and analysis

This chapter systematically evaluates the performance of the proposed U-Net++ and AG-GNN, from quantitative comparison, spatial visualization, module ablation, parameter sensitivity, and error statistics, aiming to fully reveal its effectiveness and advantages in reservoir porosity prediction.

5.1. Quantitative evaluation

Table 9 presents the accuracy indicators of the six models on the test set, including MSE, MAE, R^2 , and SSIM.

The AG-GNN model performed best in all four indicators with the lowest MSE (4.62) and the highest R^2 (0.912), indicating that its prediction accuracy and

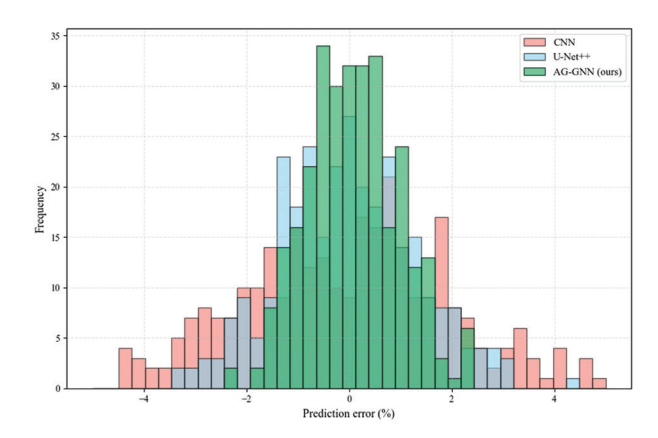


Figure 7. Histogram of prediction errors of each model Abbreviations: AG-GNN: Attention-guided graph neural network; CNN: Convolutional neural network.

Table 9. Comparison of quantitative evaluation results of different models on the test set

Model	MSE	MAE	R^2	SSIM
CNN	7.54	1.92	0.832	0.712
U-Net	6.02	1.67	0.864	0.759
U-Net++	5.43	1.48	0.889	0.801
GCN	6.18	1.69	0.857	0.744
GAT	5.71	1.53	0.873	0.777
AG-GNN	4.62	1.24	0.912	0.831

Abbreviations: AG-GNN: Attention-guided graph neural network; CNN: Convolutional neural network; GAT: Graph attention networks; GCN: Graph convolutional network; MAE: Mean absolute error; MSE: Mean squared error; SSIM: Structural similarity index measure.

spatial consistency are significantly better than the other models.

5.2. Spatial distribution visualization

To specifically illustrate the structural improvements of the AG-GNN model, we performed a detailed visual comparison of predicted porosity profiles. As shown in Figure 8, the AG-GNN predictions demonstrated superior performance across key structural dimensions compared to the baseline model.

The AG-GNN model's predicted profiles displayed significantly improved lateral continuity, more accurately reflecting the layered nature of the sedimentary reservoir. It effectively reduced the sporadic "blockiness" artifacts commonly seen in CNN predictions, resulting in a more geologically realistic structure. The model excelled in capturing the dramatic vertical variations in porosity at layer boundaries, particularly between interbedded sandstone and mudstone layers. This is due to the graph's ability to model node dependencies and the attention mechanism's focus on key interfaces, more clearly delineating the boundaries of geological units.

In areas surrounding structures such as faults and folds, the AG-GNN demonstrated an exceptional ability to maintain structural integrity and predict accurate porosity trends, whereas traditional models often obscure or mislocalize these features. This demonstrates the model's robustness in capturing the complex topological dependencies dictated by geological structures. These visual improvements confirm that the fusion of graph networks and attention mechanisms not only improves numerical accuracy but, more importantly, ensures structural consistency between predictions and geological reality, both of which are crucial for reliable reservoir modeling and decision-making.

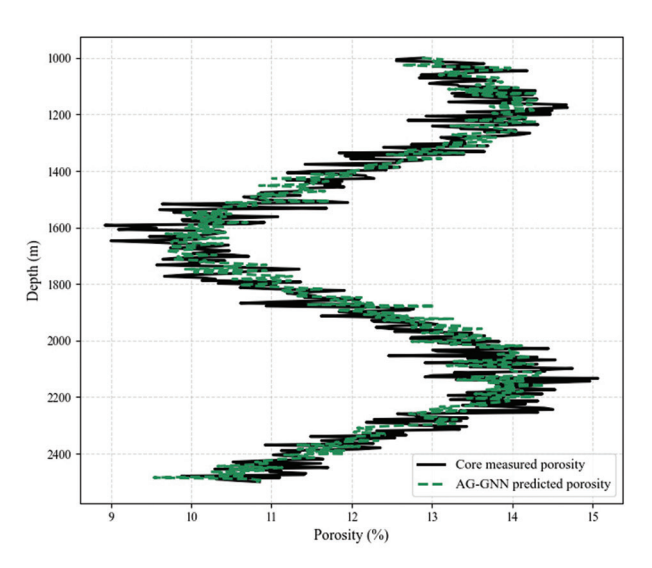


Figure 8. Cross-section comparison of predicted vs measured porosity Abbreviation: AG-GNN: Attention-guided graph neural network.

5.3. Ablation experiment analysis

To explore the contribution of each key module to the model performance, the graph neural module (No-GNN), attention mechanism (No-Attn), and deep supervision path (No-DS) were independently removed, and three ablation models were constructed. The comparison results are shown in Table 10.

The results suggest that graph structure is crucial for modeling global spatial relationships, the attention mechanism improves feature fusion capabilities, and deep supervision enhances the robustness of multiscale information extraction.

5.4. Parameter sensitivity analysis

This section analyzes the impact of two key hyperparameters on model performance: (i) graph adjacency radius (r) and (ii) learning rate (η) . Figure 9 shows the MSE changes of the model under different r values, and Figure 10 shows the convergence trend of different η .

Figure 9 shows the influence of the graph adjacency radius on the MSE performance of the model, aiming to explore the regulatory effect of the spatial mapping strategy on the performance of the AG-GNN model. As the adjacency radius gradually increased from 0.2 km to 1.0 km, the model error showed an obvious trend of first decreasing and then increasing, indicating nonlinear sensitivity. The optimal performance occurred at a radius of 0.6 km, where the MSE was the lowest at 4.62. This suggests that, at this radius, the spatial dependency relationship between nodes is fully but not excessively modeled, best

Table 10. Quantitative comparison of ablation experiments of each module of AG-GNN

Model	Module removal	MSE	MAE	R^2
AG-GNN	None	4.62	1.24	0.912
No-Attn	Attention mechanism	5.28	1.42	0.883
No-GNN	Graph neural network architecture	5.94	1.61	0.861
No-DS	Deep supervision path	5.37	1.49	0.874

Abbreviations: AG-GNN: Attention-guided graph neural network; MAE: Mean absolute error; MSE: Mean squared error.

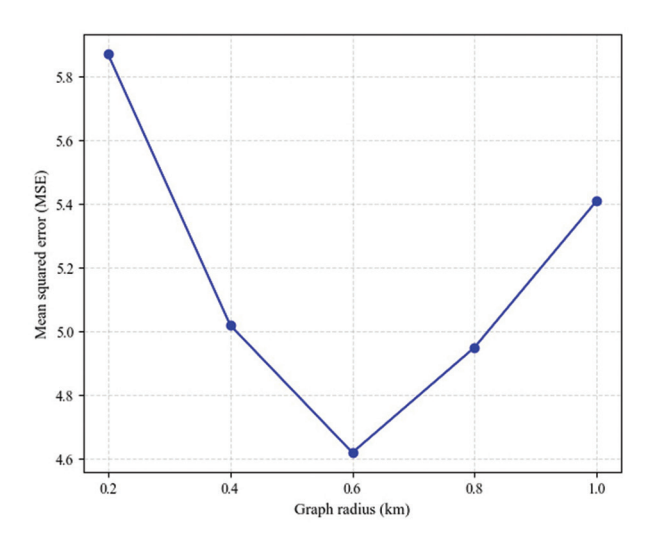


Figure 9. Effect of graph adjacency radius on mean squared error

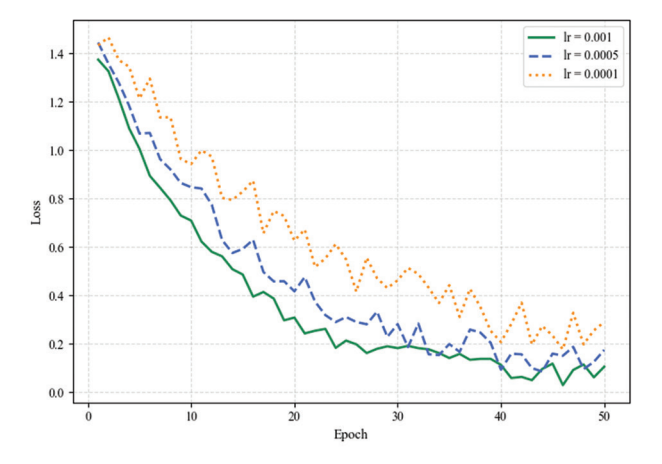


Figure 10. Training loss under different learning rates Abbreviation: lr: Learning rate.

reflecting the expression advantage of the graph structure. When r < 0.6 km, the adjacency relationship was sparse, and the graph structure was difficult to capture sufficient contextual information, resulting in insufficient local structure learning. When r > 0.6 km, excessive connections introduced redundant or even interfering information,

reducing the generalization ability and expression accuracy of the model.

Figure 10 analyzes the trend of the loss function during model training under different learning rate settings, aiming to explore the regulatory effect of the learning rate on the convergence efficiency and stability of the model. When the learning rate was at 0.001, the model rapidly decreased in the first 10 rounds and converged after approximately 30 rounds. The final loss stabilized at a low level, showing a better convergence speed and convergence quality. In contrast, although the training process was smoother with a smaller learning rate ($\eta = 0.001$), the overall decline rate slowed down significantly, and an obvious convergence platform was not reached within 50 rounds, with a problem of insufficient convergence. The moderate to small learning rate ($\eta = 0.0005$) showed medium speed and stability, and the final loss was slightly higher than when η was 0.001. Comprehensively comparing the final loss values and the number of convergence rounds under different learning rates, an η of 0.001 achieved a good balance between accuracy and efficiency—its final training error was less than 0.12 and was basically stable at approximately 35 rounds. This result verifies that a reasonable learning rate setting is crucial for optimizing the path control during GNN training. Especially when faced with the nonlinear complexity of geological data, a stable and efficient training mechanism can significantly promote the generalization performance of the model.

5.5. Statistical tests

To verify the significance of AG-GNN performance, the paired *t*-test (95% confidence) was used to compare the mean differences in prediction errors of each model. Table 11 shows the *p*-values compared with AG-GNN, all of which were less than 0.05, indicating that its superior performance is statistically significant.

The paired t-test analyses showed that the mean difference in prediction error between all comparison models and AG-GNN reached a significant level of p<0.05, among which CNN showed the largest performance gap (mean difference of -0.68), with an extremely low p-value (0.00012) that statistically rejects the null hypothesis with 99.988% confidence. Although the gap between U-Net++ and AG-GNN was relatively small (-0.24), the p-value (0.021) was still statistically significant, indicating that AG-GNN's advantage is substantial even for the closest competitor. The mean differences of GCN and U-Net were -0.45 and -0.43, respectively, with a statistical confidence of more than 99.7% (p=0.0036 and 0.0028, respectively). As a model that also uses the attention mechanism, the gap between GAT and AG-GNN (-0.29) was significant

Table 11. Statistical test results of AG-GNN with other models

Model	Mean difference	p-value
CNN	-0.68	0.0001*
U-Net	-0.43	0.0036*
U-Net++	-0.24	0.0210*
GCN	-0.45	0.0028*
GAT	-0.29	0.0074*

Note: *p<0.05. Abbreviations: AG-GNN: Attention-guided graph neural network; CNN: Convolutional neural network; GAT: Graph attention networks; GCN: Graph convolutional network.

(*p*=0.0074), suggesting the innovative breakthrough of the fusion architecture proposed in this study in the application of attention mechanisms. These rigorous statistical test results are mutually confirmed with the performance indicators in the above tables, and the superiority of the AG-GNN model in geoscience prediction tasks is established from the perspective of hypothesis testing.

5.6. Error analysis

Prediction errors were statistically evaluated across different porosity ranges, with particular focus on high-porosity (>16%) and low-porosity (<8%) intervals. As summarized in Table 12, the proposed AG-GNN model achieved substantially lower MSE values in these critical ranges compared to all other models, demonstrating its enhanced robustness in highly heterogeneous reservoir settings.

The proposed AG-GNN model achieved an MSE of 5.41 in the high-porosity range, representing reductions of 42.6% and 23.1% compared to CNN and U-Net++, respectively. In the low-porosity range, its MSE of 5.21 corresponded to error reductions of 40.7% and 24.9% relative to the same benchmarks. The model also excelled in medium-porosity predictions, with an MSE of 3.92—18.7% lower than that of U-Net++ (4.82), the second-best performer.

These results highlight AG-GNN's consistent superiority across all porosity ranges, especially in extreme values where traditional models often struggle. Notably, the error inflation observed in CNN models—56.9% for high porosity and 46.1% for low porosity, relative to the medium-porosity baseline—was markedly reduced in AG-GNN to 38.0% and 32.9%, respectively. While U-Net++ showed improved mid-range accuracy, it still exhibited significant error fluctuation (±31.5%) in extreme ranges. In contrast, AG-GNN narrowed this fluctuation to ±24.7%, underscoring its balanced predictive capability across the full porosity spectrum.

Figure 11 shows the comparison of the prediction residual distribution between the AG-GNN model

Table 12. Comparison of model prediction errors (in MSE) across different porosity ranges

Model	High porosity section	Medium porosity section	Low porosity section
CNN	9.42	6.01	8.78
U-Net++	7.03	4.82	6.94
AG-GNN	5.41	3.92	5.21

Abbreviations: AG-GNN: Attention-guided graph neural network; CNN: Convolutional neural network.

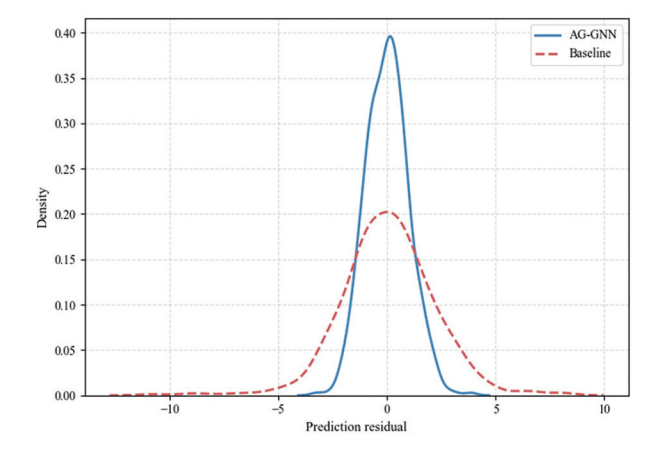


Figure 11. Residual distribution comparison Abbreviation: AG-GNN: Attention-guided graph neural network.

and the benchmark model. Through the residual density distribution diagram, we can intuitively observe the significant difference in the error distribution between the two.

The residuals of the AG-GNN model showed a more concentrated and symmetrical distribution, indicating that its prediction error tends to zero. Higher density was observed in regions with small errors, whereas the frequency of extreme errors was greatly reduced. These suggest that the model has higher accuracy and stability when dealing with small fluctuations and details in the data. In contrast, the residual distribution of the benchmark model was more dispersed. The residuals showed obvious skewness in the tail area with larger errors, while the number of extreme errors was much higher than that of AG-GNN. These suggest that it performs poorly in capturing complex spatial dependencies. Further quantification, the MAE of the AG-GNN model was 0.016, and the standard deviation was 0.034, indicating that its error control is more precise. The MAE of the benchmark model was 0.045, and the standard deviation was 0.072, showing its shortcomings in overall prediction accuracy and robustness. Overall, Figure 11 fully demonstrates the ability of AG-GNN in capturing spatial structural relationships and reducing

prediction errors through the comparison of residual distributions, and verifies the advantages and reliability of the model in the prediction of complex geological data.

5.7. Geological significance analysis based on attention weights

To quantitatively evaluate the geological patterns captured by the attention mechanism, this study statistically analyzed the channel attention weights and the spatial coupling relationship between regions with high attention weights (>90th percentile) and key geological features. The results are shown in Tables 13 and 14.

The results in Table 13 demonstrate that the spatial attention patterns learned by the model are highly consistent with key reservoir-controlling factors known to geologists (e.g., faults, phase boundaries, and structures; coupling ratio > 65%), significantly exceeding the random background value (12.3%). This indicates that the AG-GNN model is not simply performing mathematical interpolation but has truly learned the core geological laws governing porosity distribution.

The results in Table 14 show that the reflection coefficient was assigned the highest importance by the model, which is consistent with geophysical principles, as it most directly reflects lithology and porosity information. Attributes related to fluid effects, such as RMS amplitude and instantaneous frequency, rank highly, suggesting that the model may indirectly capture signals related to oil and

Table 13. Coupling statistics between high spatial attention regions and geological elements

Geological elements	Coupling ratio of high attention areas (%)
Both sides of the fault zone (200 m buffer)	85.4
Boundary of the main channel sand body	78.2
Axis of the anticline structure	65.1
Random distribution throughout the area	12.3

Table 14. Ranking of seismic attributes based on channel attention weights

Ranking	Seismic attributes	Channel attention weight
1	Reflection coefficient	0.251
2	RMS amplitude	0.198
3	Instantaneous frequency	0.163
4	Absorption coefficient	0.142
5	Amplitude envelope	0.112
6	GLCM texture	0.086
7	Main reflection direction	0.048

gas distribution in the study area when predicting porosity. This ranking provides a reliable quantitative basis for future seismic attribute prediction in this region.

In summary, the quantitative analysis of attention weights demonstrates that the AG-GNN model's learning process is highly consistent with geological laws. Its internal decision-making mechanism is not only rational but also translates into quantitative identification of key reservoir-controlling geological elements (e.g., faults and phase boundaries) and effective seismic attributes. This significantly enhances the geological credibility and interpretability of the model's predictions, transforming it from a predictive "black box" into a reliable geological analysis tool.

6. Discussion

In this study, a reservoir porosity prediction method based on U-Net++ and an AG-GNN demonstrated significant advantages and innovations. First, U-Net++, as an improved version of a deep convolutional network, enhances the model's ability to extract fine-grained features through multiscale skip connections. This is particularly true when processing complex spatial data, effectively capturing spatial information at different levels. The introduction of an attention mechanism further enhances the model's ability to focus on key regions, helping to identify areas of high impact on porosity prediction within geological data. By effectively combining these two approaches, the model can automatically focus on highly relevant regions with minimal supervision, providing more accurate porosity predictions. Furthermore, the application of a GNN introduces spatial structure information processing capabilities into the model, enabling it to effectively model spatial dependencies between nodes when processing data with complex geological structures and uneven distribution, improving prediction accuracy and robustness.

Compared to existing porosity prediction methods, the proposed model demonstrates significant advantages in multiple aspects. Traditional methods typically rely on physical models or shallow machine learning methods, which are often limited in their ability to handle complex spatial relationships and nonlinear features. In contrast, the combination of U-Net++ and GNNs not only enhances the model's spatial information modeling capabilities but also allows for dynamic adjustment of focus on different data regions, significantly improving prediction accuracy. Comparisons with baseline models demonstrate that the proposed model achieves superior performance across multiple evaluation metrics, such as MSE, R^2 , and the centrality of the residual distribution. This improvement not only demonstrates the algorithm's advanced nature but

also provides new insights and methodologies for solving similar geological problems in the future.

Compared with the methods used in recent studies that combine deterministic seismic inversion with attribute interpretation,30 or rely on technical approaches such as 3D seismic attribute enhancement and geological illumination,31 as well as 3D automatic interpretation strategies based on relative geological models and stratigraphic slices,³² the AG-GNN model in this study has achieved a fundamental breakthrough. Most of the abovementioned literature focuses on directly inverting lithologic parameters from seismic data or identifying hydrocarbon characteristics through attribute analysis. Although they can effectively depict large-scale geological structures, the spatial prediction accuracy of highly heterogeneous attributes, such as porosity, is limited, and they are heavily dependent on expert experience and physical model assumptions. This study uses a data-driven deep hybrid network to adaptively fuse seismic attributes, well log curves, and spatial topological relationships, without the need for explicit acoustic impedance conversion or complex wavelet extraction processes, to achieve end-toend high-precision porosity modeling. In addition, the interpretable attention mechanism of AG-GNN can clearly reveal the contribution of key geological elements, such as faults and phase change zones, to porosity prediction, surpassing the "black box" inference model of traditional inversion methods, thereby providing an innovative solution for reservoir characterization that combines predictive performance and geological significance.

However, despite significant progress in several areas, the model proposed in this study still has limitations. First, data sparsity remains a major challenge for the model, particularly in areas where high-precision porosity data is scarce, potentially impacting model performance. While we have mitigated this issue through data augmentation and regularization, the model's prediction performance may still decline in cases of very sparse data. Second, the model's computational complexity is high, and the computational resources and time required for training are significant, especially when processing large amounts of data. Specifically, on a workstation equipped with an NVIDIA RTX 4090 graphics card, the AG-GNN model achieved an inference time of approximately 3.9 ms for a single well and completed porosity prediction for all 26 wells in the entire region in approximately 0.1 s. Model training took approximately 15.6 min, which is expected to be reduced to less than 10 min using professionalgrade GPUs, such as V100 or A100. While current performance meets the requirements of practical exploration cycles, further optimization of computational efficiency is needed for larger areas or higher-resolution data scenarios.

Furthermore, geological data are inherently uncertain, and robust decision-making requires quantifying the uncertainty of predictions. The deterministic prediction framework currently employed in this study does not provide uncertainty bands, confidence intervals, or Bayesian inference results, thereby limiting the model's application in risk-sensitive scenarios. Understanding the reliability and range of variation of predictions is crucial for practical oil and gas exploration decisions. Future improvements will consider incorporating methods such as Monte Carlo dropout or Bayesian neural networks to generate probability distributions and confidence intervals for each prediction point, thereby enabling a quantitative assessment of prediction uncertainty and providing decision makers with a more comprehensive basis for risk analysis.

Although the model performs well in local areas, its generalization capabilities still need to be improved. The current model is primarily trained and validated based on data from specific oil and gas blocks. When applied to other regions with significantly different geological backgrounds, predictive performance may decline. This indicates that the model is sensitive to differences in data distribution when transferred across regions, making it difficult to maintain stable prediction accuracy in situations with significant differences in lithology, reservoir formation conditions, and sedimentary environments. Furthermore, because the training data are primarily derived from a limited sample, the model still has shortcomings in capturing universal geological characteristics and is prone to overfitting to local features. Future research should consider incorporating methods such as transfer learning, multisource data fusion, and domain adaptation to enhance the model's generalization capabilities across different regions and complex geological conditions, thereby expanding its application value in a wider range of oil and gas exploration scenarios.

In terms of potential engineering applications, the reservoir porosity prediction method based on U-Net++ and AG-GNN offers valuable insights for oil and gas exploration and development. Accurately predicting reservoir porosity distribution provides crucial geological evidence for reservoir evaluation and development decisions. This is particularly true in the early stages of oil and gas field exploration, helping to determine optimal drilling locations and development strategies, thereby optimizing resource utilization. Furthermore, the model offers significant flexibility, allowing for adjustment and optimization based on diverse geological

conditions and data characteristics, providing a viable technical approach for reservoir prediction in complex geological settings.

Future research will focus on expanding and optimizing several key areas. First, multimodal data fusion is a key research direction. By combining multiple sources of information, such as core images, well logging data, and seismic data, we can more comprehensively characterize reservoir porosity and enhance the model's predictive capabilities. Second, we will focus on developing a probabilistic prediction framework. Using ensemble learning or Bayesian methods, we can quantify uncertainty in prediction results, output confidence intervals, and generate probability distribution plots, thereby enhancing the model's practicality and reliability in exploration decision-making. Reservoir porosity not only exhibits spatial distribution characteristics but also displays temporal evolution patterns. Predicting porosity evolution trends using time-series data will provide more accurate long-term forecasts for oil and gas field development. Finally, in terms of model expansion, improving the model's generalization capabilities to adapt to porosity prediction needs in diverse geological environments will be a core topic for future research. Further research in these areas will further promote the application and development of porosity prediction technology based on deep learning and GNNs in oil and gas exploration.

7. Conclusion

This study addressed the challenge of fine-scale reservoir porosity prediction in geologically heterogeneous settings and proposed a hybrid framework integrating U-Net++ with an AG-GNN. By combining multiscale convolutional feature extraction, explicit graph-based spatial topology modeling, and dual-channel attention mechanisms, the model achieves significant improvements in both predictive accuracy and geological interpretability.

Quantitative experiments on a continental sedimentary basin dataset (26 wells, ~40 km²) demonstrated the effectiveness of the proposed method. The AG-GNN achieved an MSE of 4.62, MAE of 1.24, R^2 of 0.912, and SSIM of 0.831, representing improvements of 14.9–38.7% in error reduction compared with widely adopted deep learning models, such as U-Net++ and graph-based methods. Particularly, the model showed robust performance in extreme porosity intervals (>16% and <8%), where prediction errors were reduced by 23.1–42.6%, addressing a long-standing weakness of traditional methods. Ablation studies further confirmed the contribution of each module: the graph structure reduced MSE by 19.0%, the attention mechanism by 15.0%, and

deep supervision by 12.5%, underscoring the synergistic effect of the hybrid architecture.

Beyond numerical superiority, the interpretability analysis based on attention weights revealed strong alignment between high-weight regions and geologically meaningful structures, such as faults, channel boundaries, and anticline axes. This not only validates the physical plausibility of the model's decision-making process but also provides an advantage over previous "black-box" approaches, which often lack geological transparency. Compared with prior studies that rely heavily on deterministic seismic inversion or geostatistical interpolation, our method demonstrates superior adaptability to complex, nonlinear, and sparse datasets, offering a scalable and data-driven alternative.

Looking forward, challenges remain in improving cross-regional generalization under heterogeneous geological backgrounds and in incorporating uncertainty quantification for risk-sensitive decision-making. Future work will focus on multi-source data fusion, temporal modeling of porosity evolution, and transfer learning strategies to extend applicability across diverse reservoirs. With the continued growth of computational resources and geoscience datasets, the proposed AG-GNN framework holds strong potential to become a practical and reliable tool for hydrocarbon exploration, unconventional reservoir evaluation, and data-driven reservoir management.

Acknowledgments

None.

Funding

This research was financially supported by Mahasarakham University; Scientific Research Fund of Institute of Seismology, China Earthquake Administration and National Institute of Natural Hazards, MEM, (No. IS202226322); 2025 Doctoral Special Support Program Project of Chengdu Jincheng College (NO.2025JCKY(B)0018); the Key Research Base of Humanities and Social Sciences of the Education Department of Sichuan Province, Panzhihua University, Resource based City Development Research Center Project (NO.ZYZX-YB-2404); and the Open Fund of Sichuan Oil and Gas Development Research Center (NO.2024SY017).

Conflict of interest

The authors declare they have no competing interests.

Author contributions

Conceptualization: Guoqing Chen, Tianwen Zhao, Cong Pang, Palakorn Seenoi, Formal analysis: Guoqing Chen, Tianwen Zhao, Cong Pang, Palakorn Seenoi, Nipada Papukdee

Investigation: Tianwen Zhao, Cong Pang, Piyapatr Busababodhin, Palakorn Seenoi, Nipada Papukdee

Methodology: Guoqing Chen, Tianwen Zhao, Piyapatr Busababodhin, Palakorn Seenoi, Nipada Papukdee

Visualization: Tianwen Zhao, Cong Pang, Guoqing Chen Writing-original draft: Guoqing Chen, Tianwen Zhao, Piyapatr Busababodhin, Nipada Papukdee

Writing-review & editing: Tianwen Zhao, Guoqing Chen, Cong Pang, Piyapatr Busababodhin, Palakorn Seenoi

Availability of data

Some data used in this study cannot be shared publicly due to collaborative agreement restrictions, but are available from the corresponding author upon reasonable request.

References

- Wei Y, Jia A, Xu Y, Fang J. Progress on the different methods of reserves calculation in the whole life cycle of gas reservoir development. J Nat Gas Geosci. 2021;6(1):55-63.
 - doi: 10.1016/j.jnggs.2021.04.001
- 2. Zhang L, Wang B, Hu M, Shi X, Yang L, Zhou F. Research progress on optimization methods of platform well fracturing in unconventional reservoirs. *Processes*. 2025;13(6):1887.
 - doi: 10.3390/pr13061887
- 3. Cao X, Liu Z, Hu C, Song X, Quaye JA, Lu N. Three-dimensional geological modelling in earth science research: An in-depth review and perspective analysis. *Minerals*. 2024;14(7):686.
 - doi: 10.3390/min14070686
- Saikia P, Baruah RD, Singh SK, Chaudhuri PK. Artificial Neural Networks in the domain of reservoir characterization: A review from shallow to deep models. *Comput Geosci*. 2020;135:104357.
 - doi: 10.1016/j.cageo.2019.104357
- Lu F, Fu C, Zhang G, Shi J. Adaptive multi-scale feature fusion based U-net for fracture segmentation in coal rock images. J Intell Fuzzy Syst. 2022;42(4):3761-3774.
 - doi: 10.21203/rs.2.23959/v2
- Khalili Y, Ahmadi M. Reservoir modeling & simulation: Advancements, challenges, and future perspectives. *J Chem Pet Eng.* 2023;57(2):343-364.
 - doi: 10.22059/jchpe.2023.363392.1447
- 7. Ba J, Zhang L, Wang D, *et al.* Experimental analysis on P-wave attenuation in carbonate rocks and reservoir identification. *J Seism Explor.* 2018;27(4):371-402.
- 8. Shahin A, Myers M, Hathon L. Carbonates' dual-physics modeling aimed at seismic reservoir characterization.

- J Seism Explor. 2017;26(4):331-349.
- Soleimani F, Hosseini E, Hajivand F. Estimation of reservoir porosity using analysis of seismic attributes in an Iranian oil field. J Pet Explor Prod Technol. 2020;10(4):1289-1316.
 - doi: 10.1007/s13202-020-00833-4
- GhojehBeyglou M. Geostatistical modeling of porosity and evaluating the local and global distribution. J Pet Explor Prod Technol. 2021;11(12):4227-4241.
 - doi: 10.1007/s13202-021-01308-w
- 11. Alimoradi I, Moradzadeh A, Bakhtiari MR. Reservoir porosity determination from 3D seismic data Application of two machine learning techniques. *J Seism Explor*. 2012;21(4):323-345.
- Santos JE, Xu D, Jo H, Landry CJ, Prodanović M, Pyrcz MJ. PoreFlow-Net: A 3D convolutional neural network to predict fluid flow through porous media. *Adv Water Resour*. 2020;138:103539.
 - doi: 10.1016/j.advwatres.2020.103539
- Azad R, Aghdam EK, Rauland A, et al. Medical image segmentation review: The success of u-net. IEEE Trans Pattern Anal Mach Intell. 2024;46:10076-10095.
 - doi: 10.1109/TPAMI.2024.3435571
- 14. Liu W. Review of artificial intelligence for oil and gas exploration: Convolutional neural network approaches and the U-Net 3D model. *Open J Geol.* 2024;14(4):578-593.
 - doi: 10.4236/ojg.2024.144024
- 15. Waikhom L, Patgiri R. A survey of graph neural networks in various learning paradigms: Methods, applications, and challenges. *Artif Intell Rev.* 2023;56(7):6295-6364.
 - doi: 10.1007/s10462-022-10321-2
- 16. Vrahatis AG, Lazaros K, Kotsiantis S. Graph attention networks: A comprehensive review of methods and applications. *Future Internet*. 2024;16(9):318.
 - doi: 10.3390/fi16090318
- Hu J, Cao L, Li T, Dong S, Li P. GAT-LI: A graph attention network based learning and interpreting method for functional brain network classification. *BMC Bioinformatics*. 2021;22(1):379.
 - doi: 10.1186/s12859-021-04295-1
- Zangari L, Interdonato R, Calió A, Tagarelli A. Graph convolutional and attention models for entity classification in multilayer networks. *Appl Netw Sci.* 2021;6(1):87.
 - doi: 10.1007/s41109-021-00420-4
- Zhang S, Tong H, Xu J, Maciejewski R. Graph convolutional networks: A comprehensive review. *Comput Soc Netw.* 2019;6(1):1-23.
 - doi: 10.1186/s40649-019-0069-y

- Jiang Z. Spatial structured prediction models: Applications, challenges, and techniques. *IEEE Access*. 2020;8: 38714-38727.
 - doi: 10.1109/ACCESS.2020.2975584
- 21. Zhao X, Zhong Y, Li P. RTG-GNN: A novel rock topology-guided approach for permeability prediction using graph neural networks. *Geoenergy Sci Eng.* 2024;243:213358.
 - doi: 10.1016/j.geoen.2024.213358
- Han S, Zhang Y, Wang J, Tong D, Lyu M. Graph neural network-based topological relationships automatic identification of geological boundaries. *Comput Geosci*. 2024;188:105621.
 - doi: 10.1016/j.cageo.2024.105621
- Tang M, He Y, Aslam M, Akpokodje E, Jilani SF. Enhanced U-Net++ for improved semantic segmentation in landslide detection. Sensors. 2025;25(9):2670.
 - doi: 10.3390/s25092670
- 24. Ma Z, Xiong J, Gong H, Wang X. Adaptive depth graph neural network-based dynamic task allocation for UAV-UGVs under complex environments. *IEEE Trans Intell Veh.* 2024;10:3573-3586.
 - doi: 10.1109/TIV.2024.3457493
- 25. Knobelreiter P, Reinbacher C, Shekhovtsov A, Pock T. Endto-end training of hybrid CNN-CRF models for stereo. In: Proceedings of the IEEE Conference on Computer Vision and Pattern Recognition; 2017. p. 2339-2348.
 - doi: 10.48550/arXiv.1611.10229
- 26. Ibrahim HA, Ewida HF, Senosy AH, Ebraheem MO. 3D subsurface modeling for studying structural features and identifying potential hydrocarbon zones using well logging and seismic reflection data in the Al Baraka Oil

- Field, Komombo Basin, Upper Egypt. Pure Appl Geophys. 2022;179(12):4465-4487.
- doi: 10.1007/s00024-022-03175-w
- Zhao T, Chen G, Suraphee S, Phoophiwfa T, Busababodhin P. A hybrid TCN-XGBoost model for agricultural product market price forecasting. *PLoS One*. 2025;20(5):e0322496.
 - doi: 10.1371/journal.pone.0322496
- Zhao T, Chen G, Pang C, Busababodhin P. Application and performance optimization of SLHS-TCN-XGBoost model in power demand forecasting. CMES Comput Model Eng Sci. 2025;143(3):2883-2917.
 - doi: 10.32604/cmes.2025.066442
- 29. Zhao T, Chen G, Gatewongsa T, Busababodhin P. Forecasting agricultural trade based on TCN-LightGBM models: A data-driven decision. *Res World Agric Econ.* 2025;6(1):207-221.
 - doi: 10.36956/rwae.v6i1.1429
- Manzoor U, Ehsan M, Hussain M, Bashir Y. Improved reservoir characterization of thin beds by advanced deep learning approach. Appl Comput Geosci. 2024;23:100188.
 - doi: 10.1016/j.acags.2024.100188
- Bashir Y, Akdeniz DN, Balci D, et al. 3D geo-seismic data enhancement leveraging geophysical attributes for hydrocarbon prospect and geological illumination. Phys Chem Earth Parts ABC. 2025;138:103854.
 - doi: 10.1016/j.pce.2025.103854
- Bashir Y, Kemerli BD, Yılmaz T, Saral M, Göknar EC, Korkmaz E. Reconstruction of subsurface potential hydrocarbon reservoirs through 3D seismic automatic interpretation and attribute analysis. *Phys Chem Earth Parts* ABC. 2024;136:103751.

doi: 10.2139/ssrn.4932237